International Journal of Automotive Technology, Vol. ?, No. ?, pp. ?–?(year)

Estimation of Tire Lateral Force Using Extended Kalman filter and Application to Adaptive Sliding Mode Control for Torque Vectoring.

Jinmin Kim[1)], Hyunseup Jo[1)] and Sang Won Yoon[2)*]

[1)]Department of Automotive Engineering (Automotive – Computer Convergence), Hanyang University, Seoul 04763, Korea
[2)]Department of Electrical and Computer Engineering, Seoul National University, Seoul 08826, Korea

(*Received date ; Revised date ; Accepted date*)

ABSTRACT– In motorsport, achieving stable and precise yaw rate control is important. A potential solution is the use of a Torque-Vectoring (TV) system, which independently controls each wheel to optimize torque distribution. For Formula Student vehicles, handling uncertainties and minimizing computational resources are key concerns. This paper proposes the design of a Sliding Mode Controller (SMC) as the yaw moment controller within the TV system, leveraging SMC's robustness. However, the switching term designed for robustness can cause a chattering problem. To address this, an adaptive SMC (ASMC) is introduced, which adjusts the switching gain based on estimation of lateral tire forces. These forces, influenced by slip angle, road conditions, and tire cornering stiffness, are typically estimated using conventional models like Dugoff's tire model, which assumes constant cornering stiffness and may lead to inaccuracies. To improve accuracy, an Adaptive Extended Kalman Filter (AEKF) is applied for lateral force estimation, coupled with offline optimization to adjust cornering stiffness. The proposed approach is validated through co-simulations using MATLAB/Simulink and CarMaker, including sinus and steady-state steer tests. Simulation results demonstrate improved tracking of the reference yaw rate and a significant reduction in chattering.

KEY WORDS: Adaptive sliding mode control, Cornering stiffness, Extended kalman filter, Formula Student, Lateral force, Torque vectoring

NOMENCLATURE

V_x : longitudinal velocity, m/s
V_y : lateral velocity, m/s
γ : yaw rate, rad/s
a_x : longitudinal acceleration, m/s^2
a_y : lateral acceleration, m/s^2
δ : steering angle, rad
T_d : wheel driving torque, N·m
T_b : wheel braking torque, N·m
r : effective radius of tire, m
m : vehicle mass, kg
I_z : moment of inertia about z axis, kg·m^2
l_F : distance from front axle to the center of gravity, m
l_R : distance from rear axle to the center of gravity, m
L : wheel base length, m
t : half of track width, m
h : height from ground to the center of gravity, m
C_α : cornering stiffness, N/rad
σ : relaxation length, m
μ : road friction coefficient
α : slip angle
F_x : longitudinal force between road and tire, N
F_y : lateral force between road and tire, N

SUBSCRIPTS

FL, FR, RL, RR: front left, front right, rear left, rear right

1. INTRODUCTION

Vehicle's performance of acceleration, handling, and endurances are critical in racing, with high-speed cornering stability being essential. To enhance handling performance in four In-wheel drive systems, it is effective to control each motor individually for optimal torque distribution (Shino et al; 2001). This system is known as Torque-Vectoring (TV) system, requiring the design of a yaw moment controller and various control strategies can be employed for this purpose. However, for Formula student (FS) vehicle applications, we have two key considerations: robustness and low computational

* *Corresponding author*. e-mail: swyoon@snu.ac.kr

power. The driving environment is subject to affected by various disturbances. Due to some aspects of driving dynamics cannot be fully sensed in real time, it remains uncertain. Even under these conditions, the control system must act robustly. Additionally, FS vehicles may be limited in their ability to use high-performance microcontroller. Considering these conditions a Sliding Mode Controller (SMC) is utilized in this study.

Depending on which order of the sliding surface being controlled, it referred to as First-Order Sliding Mode (FOSM) and Second Order Sliding Mode (SOSM). FOSM is simple to design and requires low computational power, but it can cause chattering problems, where the input value oscillates that can cause critical problem in the system. On the other hand, SOSM effectively mitigates chattering issues and is therefore commonly applied in TV systems (Liang *et al*., 2020). For FS, we consider low computational power. Additionally, FOSM, when combined with methods to reduce chattering, provides sufficient performance for TV (de Carvalho Pinheiro *et al*, 2023). Due to switching term that used for robustness making chattering problem. One of the mitigate chattering methods is using adaptively change switching gain during the system operation, as know Adaptive Sliding Mode Control (ASMC) (Back *et al*., 2016). Therefore, if the switching term is adaptively changed based on the estimation of uncertainties, chattering can be prevented when uncertainties are low.

This uncertainty estimation is concluded to estimation of lateral tire forces, which are influenced by various factors such as slip angle, road conditions, vertical load, and the tire's cornering stiffness. Given the complexity of these interactions, precise modeling techniques are necessary for reliable force estimation. Dugoff's tire model is one of the commonly used approach due to its simplicity in combining both lateral and longitudinal tire forces based on slip angle and slip ratio. However, one major limitation of this model is the assumption that cornering stiffness remains constant, which can lead to inaccuracies in lateral force estimation, especially at higher slip angles where the tire's behavior deviates from the model's assumptions. (Dugoff *et al*., 1970).

Thus, this study is divided into two main parts. (1) Adaptive Extended Kalman Filter (AEKF) for lateral force estimation, coupled with an offline optimization approach to adjust cornering stiffness for more responsive to varying conditions. (2) TV system, which is following neutral steer yaw rate using ASMC that adjusts the switching gain based on uncertainty estimated by AEKF. Experiments were conducted in the CarMaker to validate both the AEKF and ASMC approaches.

2. ESTIMATION OF LATERAL TIRE FORCE

In this section, we describe the lateral force estimation process using an Adaptive Extended Kalman Filter (AEKF) and introduce an offline optimization approach for modifying cornering stiffness. Lateral forces are influenced by various factors, including slip angle, road conditions, vertical load on the tire, and tire's cornering stiffness. The estimation process consists of three main parts: (1) the vehicle lateral dynamics model under the three degrees of freedom (3-DoF), (2) vertical force calculation, and (3) a brief explanation of Dugoff's tire model, which is widely used for its simplicity. However, Dugoff's tire model assumes that cornering stiffness as a constant value, this can lead to inaccurate results in overall estimation as the slip angle increases.

To address this, an offline optimization approach is utilized to modify cornering stiffness, allowing it to more accurately represent the changing conditions as the slip angle increases. This is achieved through an axle distribution-based lateral force calculation method. The detailed full-wheel vehicle model is illustrated in Figure 1, and the equations of vehicle dynamics are formulated as follows (Doumiati *et al.*, 2011; Lee *et al*., 2018):

$$\begin{aligned}\dot{V}_x = \frac{1}{m}\{&F_{x,FL}\cos(\delta_{FL}) + F_{x,FR}\cos(\delta_{FR}) - \cdots \\ &F_{y,FL}\sin(\delta_{FL}) - F_{y,FR}\sin(\delta_{FR}) + F_{x,RL} + \cdots \\ &F_{x,RR} - C_{air}V_x{}^2\} + V_y\gamma\end{aligned} \tag{1}$$

$$\begin{aligned}\dot{V}_y = \frac{1}{m}\{&F_{x,FL}\sin(\delta_{FL}) + F_{x,FR}\sin(\delta_{FR}) + \cdots \\ &F_{y,FL}\cos(\delta_{FL}) + F_{y,FR}\cos(\delta_{FR}) + \cdots \\ &F_{y,RL} + F_{y,RR}\} + V_x\gamma\end{aligned} \tag{2}$$

$$\begin{aligned}\dot{\gamma} = \frac{1}{I_z}[&l_F\{F_{x,FL}\sin(\delta_{FL}) + F_{x,FR}\sin(\delta_{FR}) + \cdots \\ &F_{y,FR}\cos(\delta_{FL}) + F_{y,FR}\cos(\delta_{FR})\} - \cdots \\ &l_R(F_{y,RL} + F_{y,RR}) + \cdots \\ &t\{F_{x,FL}\cos(\delta_{FL}) - \cdots \\ &F_{x,FR}\cos(\delta_{FR}) - F_{y,FL}\sin(\delta_{FL}) + \ldots \\ &F_{y,FR}\sin(\delta_{FR}) + F_{x,RL} - F_{x,RR}\}]\end{aligned} \tag{3}$$

where V_x, V_y, γ, δ_{FL}, δ_{FR}, m, I_z, l_f, l_r, t, C_{air} are the longitudinal velocity, lateral velocity, yaw rate, front left wheel steering angle, front right wheel steering angle, vehicle mass, moment of inertia about yaw axis, distance from front axle to the center of gravity (CG), distance from rear axle to the CG, half of track width and aerodynamic drag resistance, respectively. Tire forces, $F_{x,i}$ and $F_{y,i}$ (i denotes the axle position) represent the longitudinal and lateral forces with the subscript (FL, FR, RL, RR).

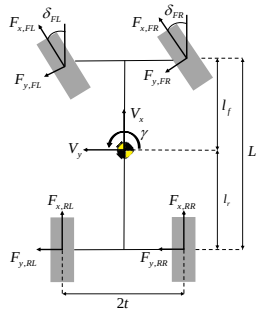

Figure 1. Representation of a four-wheel vehicle model.

Lateral forces on the tire generated by the interaction with the road surface are primarily due to the presence of a slip angle. Therefore, calculating the slip angle is critical for determining lateral tire forces; this can be calculated as described in Eq. (4).

$$\begin{aligned}
\alpha_{FL} &= \delta_{FL} - \tan^{-1}\left(\frac{V_y + l_F\gamma}{V_x}\right) \\
\alpha_{FR} &= \delta_{FR} - \tan^{-1}\left(\frac{V_y + l_F\gamma}{V_x}\right) \\
\alpha_{RL} &= -\tan^{-1}\left(\frac{V_y - l_R\gamma}{V_x}\right) \\
\alpha_{RR} &= -\tan^{-1}\left(\frac{V_y - l_R\gamma}{V_x}\right)
\end{aligned} \tag{4}$$

where δ_{FL}, δ_{FR} denotes the front left wheel steering angle and front right wheel steering angle.

2.1. Vertical tire force calculation

The vertical tire force (F_z) plays a crucial role in accurately estimating lateral forces. It is essential to account for F_z through that consider load transfer and acceleration, as these are directly influenced during the vehicle's dynamic behavior such as cornering, accelerating, and braking.

The couplings between pitch and roll dynamics are neglected in this study, assuming these have a minimal effect on the overall vertical force calculation. The vertical forces can be simplified and calculated using the approach outlined in Eq. (5) (Doumiati *et al.*, 2011).

$$\begin{aligned}
F_{z,FL} &= mg\frac{l_R}{2L} - m\frac{h}{2L}a_x - m\frac{hl_R}{tL}a_y \\
F_{z,FR} &= mg\frac{l_R}{2L} - m\frac{h}{2L}a_x + m\frac{hl_R}{tL}a_y \\
F_{z,RL} &= mg\frac{l_R}{2L} + m\frac{h}{2L}a_x - m\frac{hl_F}{tL}a_y \\
F_{z,RR} &= mg\frac{l_R}{2L} + m\frac{h}{2L}a_x + m\frac{hl_F}{tL}a_y
\end{aligned} \tag{5}$$

where m, g, h, t, L, a_x, a_y are the vehicle mass, gravitational acceleration, distance from ground to CG, half of track width, wheelbase length, longitudinal acceleration and lateral acceleration, respectively.

2.2. Dugoff's tire model

To represent tire forces, Dugoff's tire model combines both lateral and longitudinal tire forces. It calculates these forces based on the slip ratio of longitudinal forces and the slip angle for lateral forces. By neglecting longitudinal slip ratio, simplified Dugoff's tire model for lateral force is described in Eq. (6).

$$\begin{aligned}
\bar{F}_{y,i} &= -C_{\alpha,i}\tan(\alpha_i)\,f(\lambda_i) \\
f(\lambda_i) &= \begin{cases} (2-\lambda_i)\lambda_i, & \text{if } \lambda_i < 1 \\ 1, & \text{if } \lambda_i \geq 1 \end{cases} \\
\lambda_i &= \frac{\mu F_{z,i}}{2C_{\alpha,i}\,|\tan(\alpha_i)|}
\end{aligned} \tag{6}$$

where C_α represent the cornering stiffness of each axle, and μ is the tire-road friction coefficient, assumed to be 1.0 for a high-friction road surface. (Dugoff *et al*., 1970). Meanwhile, the lateral force is generated with a time lag relative to change in slip angle, it causes transient response of the tire. The lateral tire force dynamics is first order and represented as follows (Guenther *et al*., 1990, Heydinger *et al*., 1991):

$$\dot{F}_{y,i} = \frac{V_x}{\sigma_i}(-F_{y,i} + \bar{F}_{y,i}) \tag{7}$$

Here, σ denotes the relaxation length, which is assumed to be constant value of 0.1m in this study.

2.3 Axle distribution based-lateral force

As mentioned before, the Dugoff's tire model assumes that the lateral tire force is proportional to slip angle. However, this assumption is valid within a limited small range of slip angle. As slip angle increases, the behavior of the tire becomes nonlinear and no longer increases proportionally with the slip angle, instead, it approaches a saturation points where additional increases in slip angle yield diminishing in lateral force. Thus, predicting the lateral tire force using linear models becomes less accurate.

On the other hand, an alternative approach is proposed for estimating lateral tire force without relying on tire modeling and filtering methods (Li *et al*., 2019). Instead, they predict the lateral tire force directly by focusing on the distribution of vertical load across the tires relative to the total load on certain axle. The equations of the axle distribution based lateral force calculation is described in Eq. (8).

$$\tilde{F}_{y,FL} = \frac{F_{z,FL}}{F_{z,FL}+F_{z,FR}} F_{y,F}$$
$$\tilde{F}_{y,FR} = \frac{F_{z,FR}}{F_{z,FL}+F_{z,FR}} F_{y,F}$$
$$\tilde{F}_{y,RL} = \frac{F_{z,RL}}{F_{z,RL}+F_{z,RR}} F_{y,R} \quad (8)$$
$$\tilde{F}_{y,RR} = \frac{F_{z,RR}}{F_{z,RL}+F_{z,RR}} F_{y,R}$$

$$F_{y,i} = m\frac{L-l_i}{L} a_y, i = F, R \quad (9)$$

Here, $\tilde{F}_{y,i}$ represents the lateral tire force, $F_{y,F}$ and $F_{y,R}$ are the total lateral forces on the front and rear axles, respectively.

2.4. Optimization for modifying cornering stiffness

According to T. D. Gillespie, load transfer affects cornering stiffness, and this relationship can be presented by a second-order polynomial with respect to vertical force. Previous studies have also explored this relationship between cornering stiffness and vertical force (Doumiati *et al*., 2011; Jeong *et al*., 2022). The second-order polynomial equation is adjusted by adding a bias term ($C_{\alpha 0}$) in this study as described in Eq. (10), where $C_{\alpha 0}$represents the initial cornering stiffness when side slip angle is small. While the axle distribution-based method does not fully capture the nonlinear relationship between lateral force and slip angle, it remains effective for modifying the cornering stiffness and reflecting nonlinear changes as the slip angle increases.

$$C_\alpha(F_z) = aF_z^2 + bF_z + C_{\alpha 0} \quad (10)$$
$$F_{y,i} = -C_{\alpha,i}(F_{z,i}) \cdot \alpha_i \quad (11)$$

To further refine cornering stiffness, an optimization problem is then formulated aimed at reflecting the effect of vertical load, as defined in Eq. (12). This involves minimizing the sum of squared error between Eq. (8) and Eq. (11).

$$\min_{[a,b]} \sum_i \| \tilde{F}_{y,i} - (-(aF_{z,i}^2 + bF_{z,i} + C_{\alpha 0})\alpha_i) \|^2 \quad (12)$$

The Levenberg Marquardt method is utilized for this optimization task and the optimal values for the coefficients a and b as -0.006 and 3.501, respectively.

2.5. Adaptive extended kalman filter

To estimate the lateral force in state-space model, the AEKF is employed to dynamically adjust the process noise (Akhlaghi *et al*., 2017). Unlike the process noise, which is adjusted dynamically to reflect changes in the system state transitions, the measurement noise is kept constant and remain relatively stable under normal operating conditions. The AEKF utilizes 8-dimensional state vector (x_k), 5-dimensional input control vector (u_k), and 5-dimenstional measurement vector (z_k) as follows:

$$\begin{cases} x_k = [V_x, V_y, \gamma, F_{y,FL}, F_{y,FR}, F_{y,RL}, F_{y,RR}]^T \\ u_k = [\delta = \dfrac{(\delta_{FL}+\delta_{FR})}{2}, F_{x,FL}, F_{x,FR}, F_{x,RL}, F_{x,RR}]^T \\ z_k = [V_x, V_y, \gamma, a_x, a_y]^T \end{cases} \quad (13)$$

$$F_{x,i} = \frac{\tau_{d,i} - \tau_{b,i}}{r} \quad (14)$$

$F_{x,i}$ is excluded from the state vector and used as an input control vector calculated by Eq. (14). It is determined by using the wheel driving torque, wheel braking torque, and the effective radius of the tire denoted as, $\tau_{d,i}, \tau_{b,i}, r$, respectively. The priori state $(\hat{x}_k^-)$ of AEKF is calculated by integrating over discrete time deviation (Δt) as described in Eq. (15) ~ (16).

$$\hat{x}_k^- = f(\hat{x}_{k-1}, u_k) \quad (15)$$

$$f = \begin{bmatrix} \frac{1}{m}\{F_{x,FL}\cos(\delta_{FL}) + F_{x,FR}\cos(\delta_{FR}) - \cdots \\ F_{y,FL}\sin(\delta_{FL}) - F_{y,FR}\sin(\delta_{FR}) + F_{x,RL} + \cdots \\ F_{x,RR} - C_{air}V_x^2\} + V_y\gamma \\ \frac{1}{m}\{F_{x,FL}\sin(\delta_{FL}) + F_{x,FR}\sin(\delta_{FR}) + \cdots \\ F_{y,FL}\cos(\delta_{FL}) + F_{y,FR}\cos(\delta_{FR}) + F_{y,RL} + \cdots \\ F_{y,RR}\} + V_x\gamma \\ \frac{1}{I_z}[l_F\{F_{x,FL}\sin(\delta_{FL}) + F_{x,FR}\sin(\delta_{FR}) + \cdots \\ F_{y,FR}\cos(\delta_{FR}) + F_{y,FR}\cos(\delta_{FR})\} - \cdots \\ l_R(F_{y,RL} + F_{y,RR}) + t\{F_{x,FL}\cos(\delta_{FL}) - \cdots \\ F_{x,FR}\cos(\delta_{FR}) - F_{y,FL}\sin(\delta_{FL}) + \dots \\ F_{y,FR}\sin(\delta_{FR}) + F_{x,RL} - F_{x,RR}\}] \\ \frac{V_x}{\sigma}(-F_{y,FL} + \bar{F}_{y,FL}) \\ \frac{V_x}{\sigma}(-F_{y,FL} + \bar{F}_{y,FL}) \\ \frac{V_x}{\sigma}(-F_{y,FR} + \bar{F}_{y,FR}) \\ \frac{V_x}{\sigma}(-F_{y,RR} + \bar{F}_{y,RR}) \end{bmatrix} \Delta t \quad (16)$$

The measurement model is described in Eq. (17) ~ (18)

$$z_k = h(\hat{x}_k^-) + v_k \tag{17}$$

$$h = \begin{bmatrix} V_x \\ V_y \\ \gamma \\ \frac{1}{m}\{(F_{x,FL}+F_{x,FR})\cos(\delta) - \cdots \\ (F_{y,FL}+F_{y,FR})\sin(\delta) + \cdots \\ (F_{x,RL}+F_{x,RR}) - (C_{air}V_x^{\,2})\} \\ \frac{1}{m}\{(F_{x,FL}+F_{x,FR})\sin(\delta) + \cdots \\ (F_{y,FL}+F_{y,FR})\cos(\delta) + \cdots \\ (F_{y,RL}+F_{y,RR})\} \end{bmatrix} \tag{18}$$

where v_k denotes the white gaussian measurement noise and is represented as a nonlinear function of $\hat{x}_k^-$. The entire estimation process during discrete time deviation (Δt) is formulated in Eq. (16).

$$\begin{aligned} \hat{x}_k^- &= f(\hat{x}_{k-1}, u_k) \\ P_k^- &= F_k P_{k-1} F_k^{\,T} + Q_{k-1} \\ K_k &= P_k^- H_k^{\,T} (H_k P_k^- H_k^{\,T} + R)^{-1} \\ d_k &= z_k - h(\hat{x}_k^-) \\ \hat{x}_k &= \hat{x}_k^- + K_k d_k \\ Q_k &= \rho \cdot Q_{k-1} + (1-\rho)\cdot(K_k d_k d_k^{\,T} K_k^{\,T}) \end{aligned} \tag{20}$$

Here, P, Q, R are the state covariance matrix, system noise covariance, and measurement noise covariance. F, H are the Jacobian matrices of the nonlinear function of $f(\cdot)$, $h(\cdot)$ Compared to conventional EKF process, AEKF adaptively adjust the system noise covariance matrix (Q), by balancing the weight (ρ, set to 0.65) between the Q_{k-1} and the innovation (d_k) term.

3. TORQUE-VECTORING

3.1. Sliding Mode Controller Design

In this study, to ensure robustness, an Adaptive Sliding Mode Control (ASMC) approach is utilized for the yaw moment controller. To mitigate the chattering problem, an adaptive switching gain is employed. Several techniques exist to further reduce chattering, including adding a low-pass filter or replacing the signum function with a saturation function. While adding a low-pass filter can reduce chattering, it negatively impacts the controller's performance (de Carvalho Pinheiro et al., 2023). Therefore, in this study, the signum function is employed alongside the adaptive switching gain to mitigate chattering.

There are several techniques to reduce chattering, including adding a low pass filter, replacing the signum function with a saturation function, and using adaptive control gain. while adding low pass filter can reduce chattering, it negatively impacts to controller's performance. In this paper, the signum function, and adaptive control gain are employed to mitigate chattering.

To establish SMC for torque vectoring, the sliding surface is designed for the vehicle's yaw rate to track the desired yaw rate. it is expressed as follows:

$$S = \gamma - \gamma_{des} \tag{21}$$

The process of setting the control input involves following two steps. First, establish the equivalent control, which ensures $S = 0$ under the assumption of no disturbances and can be determined by imposing derivation of S is zero.

$$\dot{S} = \dot{\gamma} - \dot{\gamma}_{des} = 0 \tag{22}$$

Derivation of yaw rate is defined in Eq. (3). This equation can be partitioned into two components: one is M_x, which consist of F_x, as described in the following:

$$\begin{aligned} M_x = {} & \{F_{x,FR}\cos(\delta_{FR}) - F_{x,FL}\cos(\delta_{FL})\}t + \cdots \\ & \{F_{x,FL}\sin(\delta_{FL}) + F_{x,FR}\sin(\delta_{FR})\}l_F + \cdots \\ & (F_{x,RR} - F_{x,RL})t \end{aligned} \tag{23}$$

And the other is M_y, which consists of F_y, as described in the following:

$$\begin{aligned} M_y = {} & \{F_{y,FL}\sin(\delta_{FL}) - F_{y,FR}\sin(\delta_{FR})\}t + \cdots \\ & \{F_{y,FL}\cos(\delta_{FL}) + F_{y,FR}\cos(\delta_{FR})\}l_f - \cdots \\ & (F_{y,RR} + F_{y,RL})l_R \end{aligned} \tag{24}$$

Using above equations, eq. (24) can be substituted as follows:

$$\dot{S} = \frac{1}{I_z}(M_x + M_y + M_d) - \dot{\gamma}_{des} = 0 \tag{25}$$

where M_d is added to represent disturbances. The term M_x, which can be controlled using braking and acceleration, is treated as a control input. M_y is associated with lateral forces that are difficult to achieve. for getting equivalent control input, neglecting M_d and M_y, the equivalent control input defined Eq. (26) (Liang *et al*., 2020; de

Carvalho Pinheiro *et al.*, 2023; Zhang *et al.*, 2020; Goggia et al., 2014).

$$u_{eq} = I_z \dot{\gamma}_{des} \tag{26}$$

Originally, signum function is incorporated into the control input as a switching term. However, to reduce the chattering phenomenon, the signum function can be replaced by a saturation function (Truong *et al.*, 2013). Consequently, control input is defined as follows:

$$u = I_z \dot{\gamma}_{des} - K \cdot sat(S) \tag{27}$$

where K is the control gain for sliding mode control. To ensure the sliding surface converges in finite time, Lyapunov functions are used. According to Eq. (28). control gain must be over the $M_d + M_y$.

$$\begin{aligned} \dot{V} &= S\dot{S} \\ &= S\,[\frac{1}{I_z}(I_z \dot{\gamma}_{des} - K \cdot sat(S) + \cdots \\ &\quad M_y + M_d) - \dot{\gamma}_{des}\,] \\ &= S\,\{-\frac{K}{I_z} sat(S) + \frac{1}{I_z}(M_d + M_y)\} \\ &\le -\frac{K}{I_z} S \cdot sat(S) + \frac{|S|}{I_z}(M_d + M_y) \\ &\le |S|\{-K + M_d + M_y\} \le 0 \end{aligned} \tag{28}$$

This paper employs an adaptively adjusted switching gain, which is modified based on the results of the AEKF and the sliding surface. The AEKF results utilized to set the reference value to account for the uncertainties. However, due to the continuous oscillations observed in the AEKF output, there is a risk of using AEKF directly. To address this, the AEKF results are used as indicators that identify intervals where uncertainty is located. The corresponding equation is as follows:

$$K_{AEKF} = A\left\lceil \left| \frac{\tilde{M}_y}{A} \right| \right\rceil + B \tag{29}$$

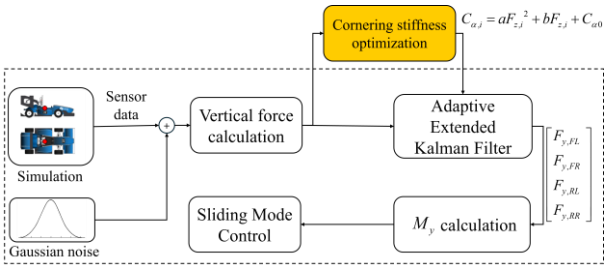

Figure 2. Overall system diagram.

where A is reference value that defines the intervals, $\tilde{M}_y$ is the estimation of M_y using AEKF B is bias term for extra disturbances.

The method of adjusting switching gain based on the states of sliding variable effectively addressed chattering phenomena near the sliding manifold (Back *et al.*, 2016). To prevent setting the excessive switching gain, a weight that reflects switching gain. This weight is managed according to the following rules:

1) If the sliding variable is smaller than in the previous step. It is assumed sliding gain is appropriate. The weight is not update
2) prevent divergence, if the sliding variable reaches a predefined maximum value, the weight is not updated.
3) If the sliding variable is larger than in the previous step, it indicates the need for a higher gain, prompting an increase in the update step.
4) If the sliding variable's sign has changed compared to the previous step, it suggests system convergence. The weight is updated to smaller

If there is a change in K_{AEKF}, it is regarded as a change in the environment. To handle this condition, the weight of switching gain is reset to 1. Following these rules, the weight update can express as follows:

$$w_t = \begin{cases} w_{t-1} & with\ |s_{t-1}| > |s_t|\ or\ w_{t-1} > 2 \\ w_{t-1} * (1-\theta) & with\ s_t s_{t-1} < 0 \\ w_{t-1} * (1+\theta) & with\ |s_{t-1}| < |s_t| \\ 1 & with\ K_{ekf,t-1} \neq K_{ekf,t} \end{cases} \tag{30}$$

where w is weight, θ is tunable variable that determines the amount of change in each step. Consequently, switching gain is Eq. (31)

$$K = w_t * K_{AEKF} \tag{31}$$

3.2. Torque Distribution

In Section 3.1, the desired momentum is generated using FOSM. To achieve this momentum, the vehicle utilizes both steering and torque distribution. The ratio of torque distribution can be calculated by optimization-based control-allocation to achieve a specific purpose (De Novovellis *et al.*, 2013) or by distributing it equally. While applying optimization-based control-allocation can enhance the vehicle's performance, this paper distributes torque equally to avoid the additional computational resources. However, the force generated by drivetrain is constrained. Therefore, if the part of more power distribution exceeded its maximum power. It

cannot maintain its speed. Due to this constraint, in that case, the excess value is redistributed to the other motor.

4. EXPERIMENT AND RESULTS

The overall process of lateral force estimation, offline cornering stiffness optimization, and torque-vectoring as illustrated in Figure 2, is tested using the CarMaker simulation environment. The tests are conducted on a Formula Student car model, equipped with virtual GNSS/IMU sensor that had Gaussian noise added to simulate real-world sensor inaccuracies, providing a more realistic evaluation of the proposed method's performance. Three distinct scenarios were employed to assess its effectiveness in estimating lateral forces and toque vectoring. The two test scenarios include:

1) Sinus steer test: this is commonly used to assess the response of a vehicle to rapidly varying steering angles. The specific conditions involved driving the vehicle at a constant speed of 40km/h, with a sinusoidal steering input ranging from $-100°$ to $100°$ over a 5-second period
2) Steady steer test: this test represents a steady-state cornering condition. The vehicle maintained a speed of 45km/h while driving on a circular track with a road curvature 45 meters.

4.1 AEKF Results

The results of estimated lateral forces and M_y during in test scenarios are shown in Figure 3 (sinus steer test) and Figure 4 (steady steer test). The root mean square error (RMSE) values are summarized in Table 1. It is observed that the RMSE values for the front lateral forces are consistently higher than lateral forces in both tests. This is attributed to front axles experience more variation due to the steering input resulting in increased errors.

Table 1. RMSE results for lateral force in each test

	$F_{y,FL}$ (N)	$F_{y,FR}$ (N)	$F_{y,RL}$ (N)	$F_{y,RR}$ (N)	M_y (Nm)
Sinus	94.73	106.11	74.44	65.71	78.24
Steady	78.22	66.75	47.22	67.93	30.63

Additionally, the RMSE values for the sinus steer test are consistently higher compared to the steady steer test. This is because sinus test involves rapid and continuous changes in the steering angle causing dynamic behavior in the overall vehicle's lateral forces.

4.2. Torque Vectoring Results

We evaluate whether the controller follows the reference yaw rate and compare the effects of torque vectoring with the baseline scenario that torque vectoring is not applied. The reference yaw rate is set according to vehicle's

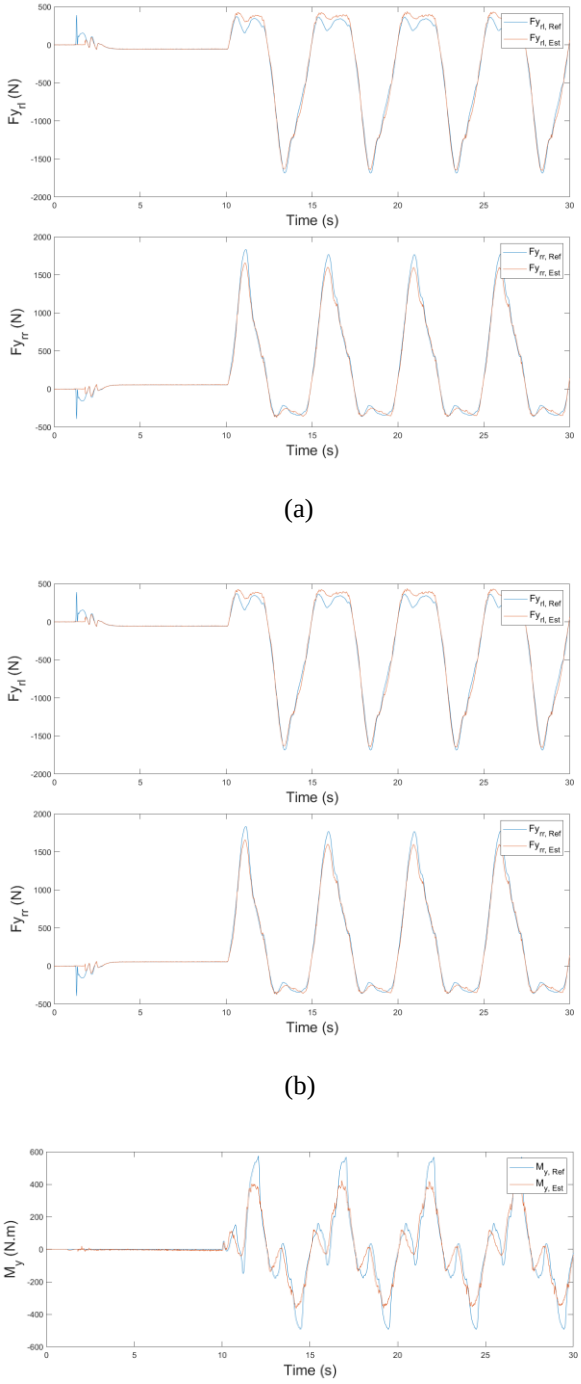

Figure 3. Estimation results for (a) front lateral force, (b) rear lateral force, and (c) M_y in sinus test.

neutral steer condition that is calculated by driver's steering angle. In this simulation, the tuning of the variable's A, B, and θ is as follows:

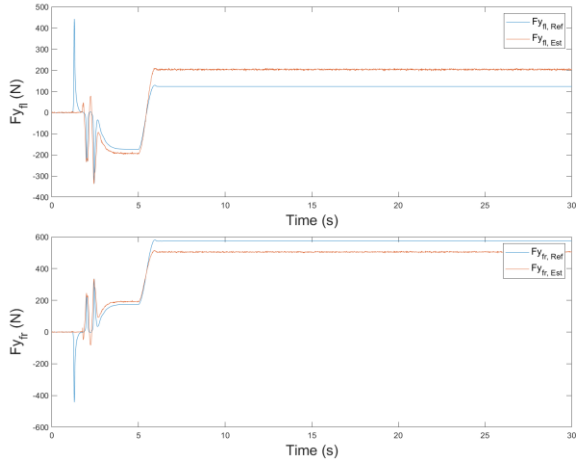

(a)

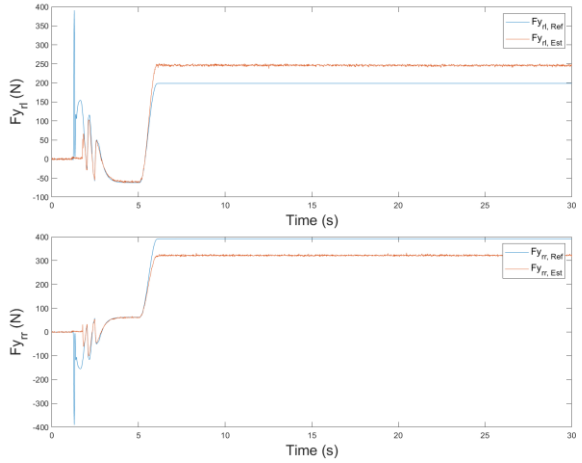

(b)

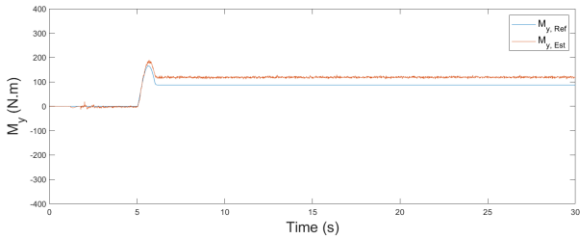

(c)

Figure 4. Estimation results for (a) front lateral force, (b) rear lateral force, and (c) M_y in steady steer test.

1) A: This parameter must be set considering the error of the AEKF. In section 4.1, the AEKF's error during both test scenarios does not exceed 500 Nm, and the adaptive term, w can make the switching gain up to double. Therefore, A is set to 500 to cover maximum 1000.
2) B: The value of B should consider the disturbance torque, M_d. However, M_d was not estimated in this paper. To ensure robustness, the control gain must be set to above this term. To achieve this, the lateral forces, and longitudinal forces that offered Carmaker are used to calculate yaw moments M_x and M_y. According to Eq. (3), the multiply by inertia moment and derivation of yaw moment comprises M_y and M_x. The differences between these values can be interpreted as M_d. Figure 5 shows the result for M_d on the, where M_d does not exceed 500Nm. Thus, B is set to 500

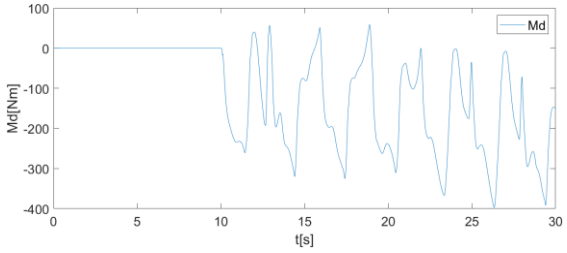

Figure 5. Results of M_d.

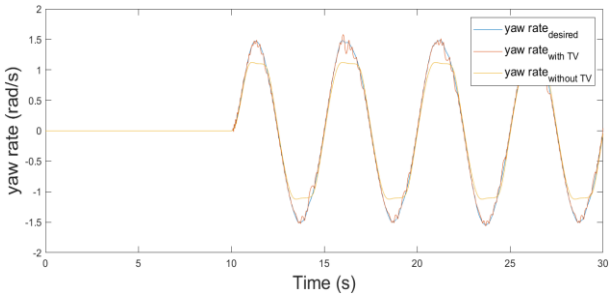

Figure 6. Yaw rate for the vehicles with and without TV system in sinus test.

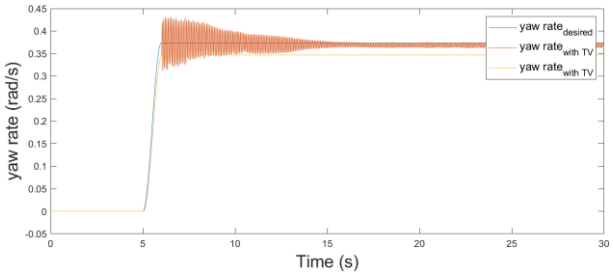

Figure 7. Yaw rate for the vehicles with and without TV system in steady steer test.

3) θ: The time step for updating the weight is set to 10 ms in this simulation. If θ is set too high, the weight changes would occur too rapidly. For stability, θ is conservatively set to 0.01 in this paper.

Figure 6 shows the results of the desired yaw rate and the vehicle's yaw rate, both with and without torque vectoring (TV) during the sinus test. Without TV, the vehicle's yaw rate is limited by its own characteristics. However, with TV, the vehicle's yaw rate closely follows the reference.

The steady-state tests results represented in Figure 7, In steady-state tests with TV, Although, there is a noticeable chattering issue, the amplitude of chattering diminishes as time progressed.

5. CONCLUSION

In this paper, a Torque-Vectoring system with an Adaptive Sliding Mode Controller (ASMC), coupled with an Adaptive Extended Kalman Filter (AEKF) for estimating tire lateral forces, was proposed to enhance handling performance in Formula Student vehicles. For the AEKF, an offline optimization method to adjust cornering stiffness was introduced to improve accuracy, and this estimation was used to adjust the switching term of the ASMC. The CarMaker results demonstrated that the AEKF provided highly accurate estimations in both the sinus and steady-state tests. The sinus test showed that the proposed controller effectively tracked the reference yaw rate. In the steady steer test, when the sliding manifold was saturated, the system maintained its states, reducing the chattering problem. The proposed adaptive algorithm proved to be capable of handling this system effectively.

ACKNOWLEDGEMENT– This work was supported by Institute of Information & communications Technology Planning & Evaluation (IITP) grant funded by the Korea government (MSIT) (No.2022-0-01053, Development of Network Load Balancing Techniques Based on Multiple Communication/Computing/Storage Resources)

REFERENCES

Doumiati, M., Victorino, A.C., Charara, A. and Lechner, D., (2010). Onboard real-time estimation of vehicle lateral tire–road forces and sideslip angle. *IEEE/ASME Transactions on Mechatronics*, **16, 4**, pp.601-614.

Lee, E., Jung, H. and Choi, S., (2018). Tire lateral force estimation using Kalman filter. *International Journal of Automotive Technology*, **19**, pp.669-676.

Dugoff, H., Fancher, P.S. and Segel, L., (1970). An analysis of tire traction properties and their influence on vehicle dynamic performance. *SAE transactions*, pp.1219-1243.

Loeb, J.S., Guenther, D.A., Chen, H.H.F. and Ellis, J.R., (1990). Lateral stiffness, cornering stiffness and relaxation length of the pneumatic tire. *SAE transactions*, pp.147-155.

Heydinger, G.J., Garrott, W.R. and Chrstos, J.P., (1991). The importance of tire lag on simulated transient vehicle response. *SAE transactions*, pp.362-374.

Li, L., d'Andréa-Novel, B. and Thorel, S., (2019), October. New online estimation algorithm of lateral tire-road coefficients based on Inertial Navigation System. In *2019 IEEE Intelligent Transportation Systems Conference (ITSC)*, pp. 3859-3866.

Jeong, D., Ko, G. and Choi, S.B., (2022). Estimation of sideslip angle and cornering stiffness of an articulated vehicle using a constrained lateral dynamics model. *Mechatronics*, **85**, p.102810.

Akhlaghi, S., Zhou, N. and Huang, Z., (2017), July. Adaptive adjustment of noise covariance in Kalman filter for dynamic state estimation. In *2017 IEEE power & energy society general meeting*, pp. 1-5.

Liang, J., Zhao, J., Dong, Z., Wang, Y. and Ding, Z.(2020). Torque Vectoring and Rear-Wheel-Steering Control for Vehicle's Uncertain Slips on Soft and Slope Terrain Using Sliding Mode Algorithm. *IEEE Transactions on Vehicular Technology* **69**, **4**, 3805-3815.

De Carvalho Pinheiro, H., Carello, M., and Punta, E. (2023). Torque vectoring control strategies comparison for hybrid vehicles with two rear electric motors. *Applied Sciences*, **13**, **14**, 8109.

Zhang, L., Ding, H., Shi, J., Huang, Y., Chen, H., Guo, K., and Li, Q. (2020). An adaptive backstepping sliding mode controller to improve vehicle maneuverability and stability via torque vectoring control. *IEEE Transactions on Vehicular Technology*, **69**, **3**, 2598-2612.

Goggia, T., Sorniotti, A., De Novellis, L., Ferrara, A., Gruber, P., Theunissen, J., Steenbeke, D., Knauder,B. and Zehetner, J. (2014). Integral sliding mode for the torque-vectoring control of fully electric vehicles: Theoretical design and experimental assessment. *IEEE Transactions on Vehicular Technology*, **64**, **5**, 1701-1715.

Truong, D. T., Meywerk, M., and Tomaske, W. (2013). Torque vectoring for rear axle using Adaptive Sliding Mode Control. *2013 international conference on control, automation and information sciences (ICCAIS)*, pp. 328-333.

De Novellis, L., Sorniotti, A.,and Gruber, P. (2013). Wheel torque distribution criteria for electric vehicles with torque-vectoring differentials. *IEEE transactions on vehicular technology*, **63**, **4**, 1593-1602.

Baek, J., Jin, M., and Han, S. (2016). A new adaptive sliding-mode control scheme for application to robot manipulators. IEEE *Transactions on industrial electronics*, **63**, **6**, 3628-3637.